Signal Processing 97 (2014) 183–194

Contents lists available at ScienceDirect

Signal Processing

journal homepage: www.elsevier.com/locate/sigpro

Rao test based cooperative spectrum sensing for cognitive radios in non-Gaussian noise ☆

Xiaomei Zhu [a,b,1], Benoit Champagne [c], Wei-Ping Zhu [d]

[a] Institute of Signal Processing Transmission, Nanjing University of Posts and Telecommunications, Nanjing 210003, China
[b] College of Electronics and Information Engineering, Nanjing University of Technology, Nanjing 211816, China
[c] Department of Electrical and Computer Engineering, McGill University, Montreal, Quebec, Canada H3A 2A7
[d] Department of Electrical and Computer Engineering, Concordia University, Montreal, Quebec, Canada H3G 1M8

ARTICLE INFO

Article history:
Received 9 August 2013
Received in revised form
23 October 2013
Accepted 28 October 2013
Available online 13 November 2013

Keywords:
Cognitive radio
Cooperative spectrum sensing
Rao detection
Decision fusion
Non-Gaussian noise

ABSTRACT

In this paper, we address the problem of spectrum sensing in the presence of non-Gaussian noise for cognitive radio networks. A novel Rao test based detector, which does not require any *a priori knowledge* about the primary user (PU) signal and channels, is proposed for the detection of a primary user in non-Gaussian noises that are molded by the generalized Gaussian distribution (GGD). The statistic of the proposed Rao detector is derived and its detection performance is analyzed in the low signal-to-noise ratio regime and compared to that of the traditional energy detection. Furthermore, the Rao-based detection is extended to a multi-user cooperative framework by using the "*k*-out-of-*M*" decision fusion rule and considering erroneous reporting channels between the secondary users and the fusion center due to Rayleigh fading. The global cooperative detection and false alarm probabilities are derived based on the cooperative sensing scheme. Analytical and computer simulation results show that for a given probability of false alarm, the Rao detector can significantly enhance the spectrum sensing performance over the conventional energy detection and the polarity-coincidence-array (PCA) method in non-Gaussian noises. Furthermore, the proposed cooperative detection scheme has a significantly higher global probability of detection than the non-cooperative scheme.

1. Introduction

In traditional fixed spectrum allocation method, most of the licensed radio spectral bands are under-utilized in time and space domains, leading to a low utilization efficiency of the frequency spectrum. Cognitive radio (CR) has emerged as a key technology that can improve the spectrum utilization efficiency in next generation wireless networks through dynamic management and opportunistic use of radio resources. In this approach, unlicensed (secondary) users (SUs) are allowed to opportunistically access a frequency band allocated to licensed (primary) user (PU), providing that the PUs are not temporally using their spectrum or they can be adequately protected from the interference created by the SUs. Hence, the radio spectrum can be reused in an opportunistic manner or shared at all time, resulting in increased capacity scaling in the network. One of the most important challenges in CR systems is to detect as reliably as possible the absence ($\mathcal{H}_0$ = null hypothesis) or presence ($\mathcal{H}_1$ = alternative hypothesis) of PU in complex environments characterized by fading effects as well as non-Gaussian noise.

Several spectrum sensing methods and algorithms have been proposed for single-user and cooperative detection under the white Gaussian noise (WGN) assumption, see e.g. [1–3]. In practice, however, the problem is more challenging

☆ This work was supported by the Scholarship Funds of Nanjing University of Technology and the National Natural Science Foundations of China under Grant 61372122.

[1] Tel.: +86 13770606907.
E-mail address: njiczxm@njut.edu.cn (X. Zhu).

0165-1684/$ - see front matter © 2013 Elsevier B.V. All rights reserved.
http://dx.doi.org/10.1016/j.sigpro.2013.10.032

as we need to detect the various PU signals impaired by non-Gaussian noise and interference, as pointed out in [4]. Non-Gaussian noise impairments may include man-made impulsive noise, co-channel interference from other SUs, emission from microwave ovens, out of band spectral leakage, etc. [5,6]. Furthermore, the performance of a spectrum detector optimized against Gaussian noise may degrade drastically when non-Gaussian noise or interference is present because of the heavy tail characteristics of its probability density function (PDF) [7,8]. In view of these problems, it is desirable to seek useful solutions to spectrum detection in practical non-Gaussian noises and to evaluate the detection performance.

Several standard models are currently available from the literature to fit non-Gaussian noise or interference distributions, such as the generalized Gaussian distribution (GGD) and the Gaussian mixture distribution (GMD). The GGD is a parametric family of distributions which can model both "heavier" and "lighter" than normal tails through the selection of its shape parameter. In particular, it has been widely used to model man-made noise, impulsive phenomena [5], and certain types of ultra-wide band (UWB) interference [9].

Spectrum sensing for CR networks in the presence of non-Gaussian noise has been addressed by several researchers recently [11–13]. However, the implementation of these detectors remains challenging as they require *a priori* knowledge of various side information, such as the variances of the channel gain between the PU and the SU and the PU signal [11], the cyclic frequency of the PU signal [12] or the variance of the receiver noise at the SU [13], which may not be readily available in practice. To overcome this limitation, [14] gives an easily implementable and nonparametric detector, namely polarity-coincidence-array (PCA), but the performance of PCA is worse than that of the energy detection when shape factor β is between 1.4 and 2. The use of the generalized likelihood ratio test (GLRT) which incorporates unknown parameter estimation to the traditional likelihood ratio test, has been proposed for local spectrum sensing in non-Gaussian noise [15]. The GLRT is an optimal detector, but it needs to perform the maximum likelihood estimation (MLE) of the unknown parameters under each hypothesis. As such, it suffers from a large computational burden.

The Rao test is an approximate form of the GLRT which only needs to estimate the unknown system model parameters under $\mathcal{H}_0$. Therefore, it has a simpler structure and lower computational complexity than the GLRT [16,17]. Although Rao test has been applied to weak signal detection in non-Gaussian noises in [16,17], its application to spectrum sensing has been limited to Gaussian noise [18]. Recently, several researchers have proposed Rao detector for signal detection in non-Gaussian noise for practical systems, but the analysis is based on the noise PDF molded by GMD considering only one or a few unknown parameters. Based on the theories of GLRT and Rao test, we use the GGD model to describe the background noise and investigate the Rao test based spectrum sensing problem in non-Gaussian noise for CR systems with unknown complex-valued PU sinal, complex-valued channel gain and noise variance. We also analyze the effect of the GGD shape parameter on Fisher information matrix (FIM) and the Rao based detection performance under the GGD noise with different shape parameters.

Multi-user cooperation is a commonly used technique in spectrum sensing due to its capability of overcoming the harmful fading and shadowing effects by employing the spatial diversity. Many recent works have exploited cooperation for improving the performance of spectrum sensing in the presence of Gaussian noise [19,20]. In these literatures, the reporting channels between SUs and FC have been assumed error-free, which is not practical. In [21,22], the detection performance has been analyzed by considering reporting errors, but the local probabilities of detection and false alarm and the cross-over probability have been assumed identical for all SUs for the reason of analytical simplicity. Furthermore, multi-user cooperation for spectrum sensing in the presence of non-Gaussian noise has not yet received much attention.

In our preliminary work [23], we have considered cooperative spectrum sensing for a CR sub-network comprised one fusion center (FC) and multiple SUs, which together seek to detect the presence/absence of a PU over a given frequency band. Each SU employs a Rao detector, which does not require any *a priori* knowledge about the PU signal and channel gains except the PDF of noise (with or without unknown variance), to independently sense the PU signal in the presence of a non-Gaussian noise characterized by the GGD. By simulations we have shown that the Rao detector outperforms the energy detector under the GGD noise with shape factor $\beta \in (0, 2]$.

In this paper, our major contributions include: (i) We derive the detection performance in terms of the probabilities of detection and false alarm for the energy detector and the Rao detector in the low SNR regime. We also analyze the detection performance when the degree of non-Gaussianity and the number of samples vary under different SNRs. (ii) We analyze and compare the performances of the two detectors in terms of the asymptotic relative efficiency (ARE) for GGD noise with various degrees of non-Gaussianity. (iii) We propose a cooperative scheme based on the local decisions of the SUs and the "*k*-out-of -*M*" decision rule. We analyze the global detection and false alarm probabilities for a more practical scenario for spectrum sensing under non-Gaussian noise where the SUs in general have different local probabilities of detection and false alarm as well as cross-over probability of erroneous reporting channels. (iv) Through theoretical analysis and numerical simulations, we show that the Rao detector can significantly enhance the local detection performance over the conventional energy detection in non-Gaussian noise and the proposed cooperative spectrum sensing scheme has a significantly higher global probability of detection than the non-cooperative one.

The rest of the paper is organized as follows. The CR system and GGD noise models under consideration are presented in Section 2. The local Rao-based detector used by the SUs is derived and analyzed in Section 3, while the theoretical performance analysis of Rao detector and energy detector for non-Gaussian noise is derived in Section 4. The cooperative spectrum sensing scheme implemented at the FC over error-free/erronous reporting channels is discussed

in Section 5. Our numerical and simulation results of the proposed schemes with comparison to the traditional energy detection are provided in Section 6. Finally, conclusions are drawn in Section 7.

Notations: $\mathbb{C}$ denotes the set of complex numbers.

2. Problem formulation

In this section, we state the spectrum sensing problem in two steps, i.e., presentation of the CR system model followed by description of the non-Gaussian noise model.

2.1. System model

We consider a CR sub-network comprised M SUs and one FC. Each SU senses the presence of the PU signal over a limited time interval, through a wireless channel that is assumed to be frequency non-selective and time invariant. The local decisions from the SUs are forwarded to an FC where a final or global decision is made. Within this general cooperative framework, spectrum sensing can be formulated as a binary hypothesis testing problem, with the null and alternative hypotheses, respectively, defined as $\mathcal{H}_0$: *PU absent* and $\mathcal{H}_1$: *PU present*.

Under these two hypotheses, the baseband signal samples $z_m(n) \in \mathbb{C}$ received by the m-th SU, where $m \in \{1, 2, \ldots, M\}$, at discrete-time $n \in \{1, 2, \ldots, N\}$, can be expressed as

$$\begin{cases} \mathcal{H}_0: & z_m(n) = w_m(n) \\ \mathcal{H}_1: & z_m(n) = u_m(n) + w_m(n) \end{cases} \tag{1}$$

where $w_m(n) \in \mathbb{C}$ is a complex-valued additive background noise present under both hypotheses and $u_m(n) \in \mathbb{C}$ is the complex-valued PU signal component present only under $\mathcal{H}_1$. Considering a time-invariant, flat fading channel model, we can express the latter as $u_m(n) = h_m s(n)$ where $s(n) \in \mathbb{C}$ is the signal sample emitted by the PU at time n and $h_m \in \mathbb{C}$ is the channel gain between the PU's transmitter and the m-th SU's receiver. Under both hypotheses, we model the noise sequence $w_m(n)$ as an independent and identically distributed (IID) random process, with zero-mean, variance σ_m^2 and circularly symmetric distribution, whose special form is further discussed below; the noise sequences observed by different SUs are mutually independent. The PU signal $s(n)$ is modeled as an IID process with zero-mean but otherwise arbitrary distribution; it is assumed to be independent of the noise processes $\{w_m(n)\}$. The channel gains h_m are assumed to be IID over the spatial index m, with zero-mean but arbitrary distribution, and they are independent of the PU signal and SU noises.

In general, the SUs have no *a priori* knowledge about the emitted PU signal $s(n)$ nor the channel gains h_m, although they can extract relevant information about the noise $w_m(n)$ through measurement under $\mathcal{H}_0$ and local processing.

2.2. Noise model

In this paper, we assume that the probability density function (PDF) of the measurement noise is known up to a variance parameter σ_m^2, which will be estimated by the SUs as part of the proposed approach. Specifically, we consider the GGD model in the context of CR, which allows to control the degree of non-Gaussianity in the noise distribution efficiently through a shape parameter.

The noise samples in practice seem to be higher in magnitude than that from the Gaussian distribution [24], in other words the PDF of impulsive non-Gaussian noise decays at a lower rate than the Gaussian. Therefore, having a tail heavier than the Gaussian distribution is a key feature of the required non-Gaussian model. The main idea behind the GGD is to retain an exponential type of decay, as in the Gaussian PDF, but to allow for varying degree of decay rate by controlling the exponent applied to its argument. This feature makes it possible to better fit various types of noise encountered in practice, such as man-made impulsive noise, co-channel interference from other CRs, and emission from microwave ovens [10].

We suppose that the non-Gaussian noise $w_m(n)$ in (1) belongs to the GGD family and is a zero-mean complex generalized Gaussian random variable with unknown variance $\sigma_{w_m}^2$, where the real and the imaginary parts of $w_m(n)$ are independent GGD random variables each with zero mean and the same variance $\sigma_{w_m}^2/2$. The PDF of the GGD with variance $\sigma_{w_m}^2 > 0$ and shape factor $\beta > 0$ is obtained from [24]

$$p\left(w_m(n); \beta, \sigma_{w_m}^2\right) = \frac{\beta^2}{[2B(\beta, \sigma_{w_m}^2/2)\Gamma(1/\beta)]^2} \times \exp\left(- \frac{|w_m^{\Re}(n)|^\beta + |w_m^{\Im}(n)|^\beta}{\left[B\left(\beta, \frac{\sigma_{w_m}^2}{2}\right)\right]^\beta} \right) \tag{2}$$

where $w_m^{\Re}(n) = \mathrm{Re}\{w_m(n)\}$ and $w_m^{\Im}(n) = \mathrm{Im}\{w_m(n)\}$ denote the real and imaginary parts of $w_m(n)$,

$$B\left(\beta, \sigma_{w_m}^2\right) = \sigma_{w_m} \left(\frac{\Gamma(1/\beta)}{2\Gamma(3/\beta)} \right)^{1/2} \tag{3}$$

is a scaling factor and $\Gamma(\alpha) = \int_0^\infty x^{\alpha-1} e^{-x}\, dx$. It is easily seen that the GGD reduces to the Gaussian distribution for $\beta = 2$ and to the Laplacian distribution for $\beta = 1$.

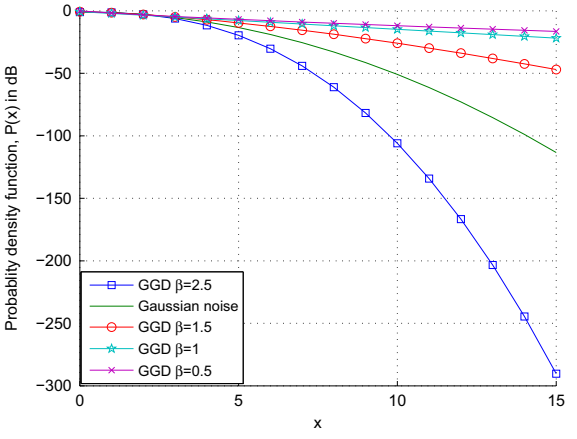

Fig. 1. PDF comparisons of Gaussian noise and GGD noise ($\sigma_{w_m}^2 = 1$).

The PDFs of the GGDs in logarithmic scale, for $\sigma^2_{w_m}=1$ and different values of the shape factor β, are plotted in Fig. 1. By varying β, different tail behaviors can be obtained: for $\beta>2$, the tail decays faster than for the normal, while for $0<\beta<2$, the tail decays more slowly and is therefore "heavier" than for the normal. So when $0<\beta<2$, the GGD can be used to fit the non-Gaussian noises in practical CR systems, and moreover a smaller value of β indicates a higher degree of non-Gaussianity.

Then, spectrum sensing for CR applications in non-Gaussian noise must take into account these large magnitude noise samples with heavier-than-normal tail distributions, in order to improve the detection performance, e.g. increasing the probability of detection under a given probability of false alarm. To this end, a good detector for non-Gaussian noise typically utilizes nonlinearities or clippers to reduce the noise spikes, as will be seen below for the proposed Rao detector.

3. Rao detector for local spectrum sensing

In this section, we propose a nonlinear detector based on the Rao test which will allow the SUs to make a preliminary, local decision on the channel occupancy by the PU. The derivation is carried on for a selected SU, say the one with index m.

Referring to the system model in (1), we begin by introducing some necessary definitions and notations for convenience in analysis. We define $u^{\Re}_m(n)=\mathrm{Re}\{u_m(n)\}$, $u^{\Im}_m(n)=\mathrm{Im}\{u_m(n)\}$, $z^{\Re}_m(n)=\mathrm{Re}\{z_m(n)\}$ and $z^{\Im}_m(n)=\mathrm{Im}\{z_m(n)\}$. The complete vector of signal samples observed by the SU is denoted as $\boldsymbol{z}_m=[z_m(1),\ldots,z_m(N)]^T$. Adopting the notations from [25], we define the parameter vector

$$\boldsymbol{\theta}_r=[u^{\Re}_m(1),\ldots,u^{\Re}_m(N),u^{\Im}_m(1),\ldots,u^{\Im}_m(N)]^T \tag{4}$$

which contains the real and imaginary parts of the PU signal samples. We also let $\theta_s=\sigma^2_{w_m}$ denote the nuisance parameter for the detection problem at hand. Finally, we define $\boldsymbol{\theta}=[\boldsymbol{\theta}_r^T\ \theta_s]^T$, which is a $(2N+1)$-dimensional real vector.

The Rao test is asymptotically equivalent to the GLRT, yet it does not require the MLE of the unknown parameters under $\mathcal{H}_1$ and is computationally simpler than GLRT [25]. In order to formulate the Rao test, we first recast the detection model (1) in the following equivalent form:

$$\begin{cases}\mathcal{H}_0: & \boldsymbol{\theta}_r=\mathbf{0}, \quad \theta_s>0\\ \mathcal{H}_1: & \boldsymbol{\theta}_r\neq\mathbf{0}, \quad \theta_s>0\end{cases} \tag{5}$$

Within this framework, the Rao test statistic $T_R(\boldsymbol{z}_m)$ at the m-th SU for composite binary parameter test can be expressed as

$$T(\boldsymbol{z}_m)=\nabla \ln p(\boldsymbol{z}_m;\boldsymbol{\theta})^T[I^{-1}(\boldsymbol{\theta})]_{rr}\nabla \ln p(\boldsymbol{z}_m;\boldsymbol{\theta})|_{\boldsymbol{\theta}=\hat{\boldsymbol{\theta}}_0} \tag{6}$$

where $p(\boldsymbol{z}_m;\boldsymbol{\theta})$ is the PDF of the received complex-valued observation vector $\boldsymbol{z}_m$ under $\mathcal{H}_1$, ∇ denotes the gradient operator with respect to the entries of vector $\boldsymbol{\theta}_r$, defined as

$$\nabla=\left[\frac{\partial}{\partial u^{\Re}_m(1)},\ldots,\frac{\partial}{\partial u^{\Re}_m(N)},\frac{\partial}{\partial u^{\Im}_m(1)},\ldots,\frac{\partial}{\partial u^{\Im}_m(N)}\right]^T, \tag{7}$$

$\hat{\boldsymbol{\theta}}_0=[\hat{\boldsymbol{\theta}}_{r0}^T\ \hat{\theta}_{s0}]^T$ is the MLE of $\boldsymbol{\theta}$ under $\mathcal{H}_0$, and $[\boldsymbol{I}^{-1}(\boldsymbol{\theta})]_{rr}$ is an $2N\times 2N$ matrix obtained as the upper-left block partition of the inverse Fisher information matrix (FIM) $\boldsymbol{I}^{-1}(\boldsymbol{\theta})$. Here the FIM $\boldsymbol{I}(\boldsymbol{\theta})$ associated to the PDF $p(\boldsymbol{z}_m;\boldsymbol{\theta})$ has the following partitioned form [26]:

$$\boldsymbol{I}(\boldsymbol{\theta})=\begin{bmatrix}\boldsymbol{I}_{rr}(\boldsymbol{\theta}) & \boldsymbol{I}_{rs}(\boldsymbol{\theta})\\ \boldsymbol{I}_{sr}(\boldsymbol{\theta}) & \boldsymbol{I}_{ss}(\boldsymbol{\theta})\end{bmatrix}, \tag{8}$$

where the upper left block $\boldsymbol{I}_{rr}(\boldsymbol{\theta})$ has a dimension $2N\times 2N$.

According to the system model defined in Section 2, the PDF of the received signal vector $\boldsymbol{z}_m$, with IID samples, can be expressed as

$$p(\boldsymbol{z}_m;\boldsymbol{\theta})=\prod_{n=1}^{N}\frac{\beta^2}{\left[2B\left(\beta,\frac{\sigma^2_{w_m}}{2}\right)\Gamma(1/\beta)\right]^2}\times\exp\left\{-\frac{|z^{\Re}_m(n)-u^{\Re}_m(n)|^\beta+|z^{\Im}_m(n)-u^{\Im}_l(n)|^\beta}{\left[B\left(\beta,\frac{\sigma^2_{w_m}}{2}\right)\right]^\beta}\right\}. \tag{9}$$

Taking the natural logarithm of (9), we obtain

$$\ln p(\boldsymbol{z}_m;\boldsymbol{\theta})=2N\ln\frac{\beta}{\left[2B\left(\beta,\frac{\sigma^2_{w_m}}{2}\right)\Gamma(1/\beta)\right]}-\frac{\sum_{n=1}^{N}(|z^{\Re}_m(n)-u^{\Re}_m(n)|^\beta+|z^{\Im}_m(n)-u^{\Im}_m(n)|^\beta)}{\left[B\left(\beta,\frac{\sigma^2_{w_m}}{2}\right)\right]^\beta} \tag{10}$$

From (5), it follows that the MLE of $\boldsymbol{\theta}_r$ under $\mathcal{H}_0$ is simply $\hat{\boldsymbol{\theta}}_{r0}=\mathbf{0}$. The MLE of $\theta_s=\sigma^2_{w_m}$ under $\mathcal{H}_0$ is found by computing the derivative of (10) with respect to $\sigma^2_{w_m}$, under $\boldsymbol{\theta}_r=\mathbf{0}$, and setting the result to zero, yielding

$$\hat{\theta}_{s0}=\hat{\sigma}^2_{w_m}=\left[\frac{\beta\left(\frac{2\Gamma(3/\beta)}{\Gamma(1/\beta)}\right)^{\beta/2}}{2N}\sum_{n=1}^{N}\left(|z^{\Re}_m(n)|^\beta+|z^{\Im}_m(n)|^\beta\right)\right]^{2/\beta} \tag{11}$$

The gradient of (10) with respect to $\boldsymbol{\theta}_r$, as defined in (7), can be expressed as

$$\nabla \ln p(\boldsymbol{z}_m;\boldsymbol{\theta})=[\boldsymbol{\nu}^{\Re}(\boldsymbol{z}_m;\boldsymbol{\theta}),\boldsymbol{\nu}^{\Im}(\boldsymbol{z}_m;\boldsymbol{\theta})]^T \tag{12}$$

where $\boldsymbol{\nu}^{\Re}(\boldsymbol{z}_m;\boldsymbol{\theta})=[\nu^{\Re}_1,\ldots,\nu^{\Re}_N]$ and $\boldsymbol{\nu}^{\Im}(\boldsymbol{z}_m;\boldsymbol{\theta})=[\nu^{\Im}_1,\ldots,\nu^{\Im}_N]$. In turn, the entries of these vectors are defined as

$$\nu^{\Re}_n=\frac{\beta|z^{\Re}_m(n)-u^{\Re}_m(n)|^{\beta-1}\mathrm{sgn}(u^{\Re}_m(n)-z^{\Re}_m(n))}{\left[B\left(\beta,\frac{\sigma^2_{w_m}}{2}\right)\right]^\beta} \tag{13}$$

$$\nu^{\Im}_n=\frac{\beta|z^{\Im}_m(n)-u^{\Im}_m(n)|^{\beta-1}\mathrm{sgn}(u^{\Im}_m(n)-z^{\Im}_m(n))}{\left[B\left(\beta,\frac{\sigma^2_{w_m}}{2}\right)\right]^\beta} \tag{14}$$

where $\mathrm{sgn}(x)$ is 1 if $x>0$ and -1 if $x\le 0$.

We now proceed to calculate the submatrix $[\boldsymbol{I}^{-1}(\boldsymbol{\theta})]_{rr}$ of $\boldsymbol{I}^{-1}(\boldsymbol{\theta})$ under $\mathcal{H}_0$, which appears in (6). Using (8) along

with the definition of the FIM in [26], we can find (see Appendix A)

$$\boldsymbol{I}_{rr}\left(\hat{\boldsymbol{\theta}}_0\right)=\frac{2\beta(\beta-1)\Gamma(1-1/\beta)\Gamma(3/\beta)}{\hat{\sigma}^2_{w_m}\Gamma^2(1/\beta)}\mathcal{I}_{2N} \tag{15}$$

where $\mathcal{I}_{2N}$ is the $2N\times 2N$ identity matrix,

$$\boldsymbol{I}_{rs}\left(\hat{\boldsymbol{\theta}}_0\right)=[\boldsymbol{I}_{sr}(\hat{\boldsymbol{\theta}}_0)]^T=-\frac{\beta^2\Gamma^{1/2}(3/\beta)}{2\hat{\sigma}^3_{w_m}\Gamma^{3/2}(1/\beta)}\mathbf{1}_{2N,1} \tag{16}$$

where $\mathbf{1}_{2N,1}$ is the $2N\times 1$ matrix of ones, and

$$\boldsymbol{I}_{ss}\left(\hat{\boldsymbol{\theta}}_0\right)=\frac{N\beta}{2\hat{\sigma}^4_{w_m}}. \tag{17}$$

Next, applying a well-known matrix inversion formula for block partitioned matrices [27], the $2N\times 2N$ upper-left block of the inverse FIM can be expressed as

$$[\boldsymbol{I}^{-1}(\hat{\boldsymbol{\theta}}_0)]_{rr}=[\boldsymbol{I}_{rr}(\hat{\boldsymbol{\theta}}_0)-\boldsymbol{I}_{rs}(\hat{\boldsymbol{\theta}}_0)\boldsymbol{I}_{ss}^{-1}(\hat{\boldsymbol{\theta}}_0)\boldsymbol{I}_{sr}(\hat{\boldsymbol{\theta}}_0)]^{-1} \tag{18}$$

Using (16) and (17), we have

$$\boldsymbol{I}_{rs}\left(\hat{\boldsymbol{\theta}}_0\right)\boldsymbol{I}_{ss}^{-1}\left(\hat{\boldsymbol{\theta}}_0\right)\boldsymbol{I}_{sr}\left(\hat{\boldsymbol{\theta}}_0\right)=\frac{\beta^3\Gamma(3/\beta)}{2N\hat{\sigma}^2_{w_m}\Gamma^3(1/\beta)}\mathbf{1}_{2N,2N} \tag{19}$$

Note that for a given β, $\beta^3\Gamma(3/\beta)/2\hat{\sigma}^2_{w_m}\Gamma^3(1/\beta)$ is a finite value and so when $N\to\infty$, (19) tends to be a zero matrix. Thus when N is very large, (18) can be approximated by

$$[\boldsymbol{I}^{-1}(\hat{\boldsymbol{\theta}}_0)]_{rr}\approx\boldsymbol{I}_{rr}^{-1}(\hat{\boldsymbol{\theta}}_0) \tag{20}$$

Finally, by substituting (11), (12) and (20) into (6), we obtain the Rao detection statistic, i.e.,

$$T_R(\boldsymbol{z}_m)=\phi(\beta)\sum_{n=1}^{N}[|z_m^{\Re}(n)|^{2(\beta-1)}+|z_m^{\Im}(n)|^{2(\beta-1)}] \tag{21}$$

where $\phi(\beta)$ is a scaling factor defined as

$$\phi(\beta)=\frac{\beta\Gamma\left(\frac{3}{\beta}\right)^{\beta-1}}{(\beta-1)\left(\frac{\hat{\sigma}^2_{w_m}}{2}\right)^{\beta-1}\Gamma\left(\frac{1}{\beta}\right)^{\beta-2}\Gamma\left(1-\frac{1}{\beta}\right)} \tag{22}$$

From (21), the statistic of Rao detector is only the function of β, so for the GGD noise with a given β, our proposed detector does not require any *a priori* knowledge of the PU signal, the channel gain and the variance of noise.

In summary, the Rao detector gives a binary decision y_m for the m-th SU as

$$y_m=\begin{cases}1, & T_R(\boldsymbol{z}_m)\geq\gamma_m\\ 0, & T_R(\boldsymbol{z}_m)<\gamma_m\end{cases} \tag{23}$$

where γ_m is a threshold, usually pre-determined according to the desired probability of false alarm requirement for the m-th SU.

4. Performance analysis

In this section, analytical expressions for the probabilities of false alarm P_{fa} and detection P_{d} of the energy detector and that of the proposed Rao test detector are derived. The asymptotic relative efficiency (ARE) of the Rao detector with respect to the energy detector is also analyzed.

4.1. Energy detection

The energy detector has the following test statistic:

$$T_{E_m}=\sum_{n=1}^{N}|z_m(n)|^2 \tag{24}$$

We assume that the number of samples N in any given sensing interval is large enough to invoke the central limit theorem (CLT). So for a sufficiently large value of N, the PDF of T_{E_m} will approach a Gaussian distribution even if the noise $w_m(n)$ is GGD. Hence, we have

$$\begin{cases}\mathcal{H}_0: & T_{E_m}\sim\mathcal{N}(E\{T_{E_m}|\mathcal{H}_0\},\text{var}\{T_{E_m}|\mathcal{H}_0\})\\ \mathcal{H}_1: & T_{E_m}\sim\mathcal{N}(E\{T_{E_m}|\mathcal{H}_1\},\text{var}\{T_{E_m}|\mathcal{H}_1\})\end{cases} \tag{25}$$

Based on the received observation complex signal in (1) under two hypotheses, we derive the expressions for the means and the variances. Before that, we give the even moments of GGD noise w as

$$\mu_w^q=\left[\frac{\Gamma(1/\beta)}{\Gamma(3/\beta)}\right]^{q/2}\frac{\Gamma((q+1)/\beta)}{\Gamma(1/\beta)}\sigma_w^q \tag{26}$$

for $q=2,4,\ldots$. Since the PDF in (2) is symmetric around zero, the odd moments of w are zero. The means under $\mathcal{H}_0$ and $\mathcal{H}_1$ can be calculated as

$$E\{T_{E_m}|\mathcal{H}_0\}=\sum_{n=1}^{N}E|w_m(n)|^2=N\sigma_m^2 \tag{27}$$

$$E\{T_{E_m}|\mathcal{H}_1\}=\sum_{n=1}^{N}E|z_m(n)|^2=N(E[|u_m|^2]+\sigma_m^2) \tag{28}$$

where $E[|u_m|^2]=E[|u_m(n)|^2]$, $n=1,2,\ldots,N$. The variance of T_{E_m} under $\mathcal{H}_0$ can be calculated as

$$\begin{aligned}\text{var}\{T_{E_m}|\mathcal{H}_0\}&=E\left(\sum_{n=1}^{N}|w_m(n)|^2-E\{T_{E_m}|\mathcal{H}_0\}\right)^2\\&=N\left(\frac{\Gamma(1/\beta)\Gamma(5/\beta)}{\Gamma^2(3/\beta)}-1\right)\sigma_m^4\end{aligned} \tag{29}$$

To obtain a closed-form expression for $\text{var}\{T_{E_m}|\mathcal{H}_1\}$, we assume that $|u_m(n)|\ll|w_m(n)|$ (the low SNR case). By using a Taylor series expansion to approximate $|u_m(n)+w_m(n)|^4$ around $w_m(n)$ [11], we can get (see Appendix B for detail)

$$\begin{aligned}\text{var}\{T_{E_m}|\mathcal{H}_1\}&=E\left(\sum_{n=1}^{N}|z_m(n)|^2-E\{T_{E_m}|\mathcal{H}_1\}\right)^2\\&=N\left[\left(\frac{\Gamma(1/\beta)\Gamma(5/\beta)}{\Gamma^2(3/\beta)}-1\right)\sigma_m^4+2E\left[|u_m|^2\right]\sigma_m^2-E^2\left[|u_m|^2\right]\right]\end{aligned} \tag{30}$$

The above expression applies to the low SNR regime. It should be mentioned that when the SNR is moderate or high the performance of our proposed Rao detector is much better than that of the energy detector, as will be shown by simulations.

With (27)–(30), $P_{\text{fa},m}$ and $P_{\text{d},m}$ can be written as

$$P_{\text{fa},m}=\Pr\{T_{E_m}>\gamma_{E_m}|\mathcal{H}_0\}=Q\left(\frac{\gamma_{E_m}-E\{T_{E_m}|\mathcal{H}_0\}}{\sqrt{\text{var}\{T_{E_m}|\mathcal{H}_0\}}}\right) \tag{31}$$

$$P_{\text{d},m}=\Pr\{T_{E_m}>\gamma_{E_m}|\mathcal{H}_1\}=Q\left(\frac{\gamma_{E_m}-E\{T_{E_m}|\mathcal{H}_1\}}{\sqrt{\text{var}\{T_{E_m}|\mathcal{H}_1\}}}\right) \tag{32}$$

where γ_{E_m} is the threshold for energy detection at the m-th CR, and $Q(x)=(1/\sqrt{2\pi})\int_x^\infty e^{-t^2/2}\,dt$. When $P_{\mathrm{fa},m}$ is given, the threshold γ_{E_m} of the energy detector is given by

$$\begin{aligned}\gamma_{E_m}&=\sqrt{\mathrm{var}\{T_{E_m}|\mathcal{H}_0\}}Q^{-1}(P_{\mathrm{fa},m})+E\{T_{E_m}|\mathcal{H}_0\}\\&=\left\{\sqrt{N\left[\frac{\Gamma(1/k)\Gamma(5/k)}{\Gamma^2(3/k)}-1\right]}Q^{-1}(P_{\mathrm{fa},m})+N\right\}\sigma_m^2\end{aligned}\tag{33}$$

By substituting (28), (30) and (33) into (32), the probability of detection of the energy detector is finally obtained as

$$P_{\mathrm{d},m}=Q\left(\frac{\sqrt{\left(\frac{\Gamma(1/\beta)\Gamma(5/\beta)}{\Gamma^2(3/\beta)}-1\right)}Q^{-1}(P_{\mathrm{fa},m})-\sqrt{N}\zeta_m}{\sqrt{\left(\frac{\Gamma(1/\beta)\Gamma(5/\beta)}{\Gamma^2(3/\beta)}-1\right)+2\zeta_m-\zeta_m^2}}\right)\tag{34}$$

where $\zeta_m=E[|u_m|^2]/\sigma_m^2$.

4.2. Rao test detection

As $N\to\infty$, the asymptotic PDF of the Rao test statistic will be the same as for GLRT statistic [25]. Hence, we have

$$T_R(z_m)\sim\begin{cases}\mathcal{X}^2_{2N} & \text{under } \mathcal{H}_0\\ \mathcal{X}'^2_{2N}(\lambda) & \text{under } \mathcal{H}_1\end{cases}\tag{35}$$

where $\mathcal{X}^2_r$ denotes a chi-squared PDF with $2N$ degrees of freedom, and $\mathcal{X}'^2_r(\lambda)$ denotes a non-central chi-squared PDF with $2N$ degrees of freedom and non-centrality parameter λ as given by

$$\lambda=\boldsymbol{\theta}_{r1}^T[I_{rr}(\hat{\boldsymbol{\theta}}_0)-I_{rs}(\hat{\boldsymbol{\theta}}_0)I_{ss}^{-1}(\hat{\boldsymbol{\theta}}_0)I_{sr}(\hat{\boldsymbol{\theta}}_0)]\boldsymbol{\theta}_{r1}\tag{36}$$

where $\boldsymbol{\theta}_{r1}$ is the value of $\boldsymbol{\theta}_r$ under $\mathcal{H}_1$. By substituting (15) and (19) into (36), we have

$$\lambda\approx\frac{2\beta(\beta-1)\Gamma(1-1/\beta)\Gamma(3/\beta)}{\sigma_w^2\Gamma^2(1/\beta)}\sum_{n=1}^{N}|u_m(n)|^2\tag{37}$$

and its mean $\bar{\lambda}$ is given by

$$\bar{\lambda}=E[\lambda]=N\frac{2\beta(\beta-1)\Gamma(1-1/\beta)\Gamma(3/\beta)}{\Gamma^2(1/\beta)}\zeta_m\tag{38}$$

Using (35) and the non-centrality parameter $\bar{\lambda}$, one can obtain the PDF of $T_R(z_m)$ as

$$p(t_m)=\begin{cases}\dfrac{1}{2^N\Gamma(N)}t_m^{N-1}\exp\left(-\dfrac{t_m}{2}\right) & \text{under } \mathcal{H}_0\\ \dfrac{1}{2}\left(\dfrac{t_m}{\bar{\lambda}}\right)^{(N-1)/2}\exp\left[-\dfrac{1}{2}(t_m+\bar{\lambda})\right]I_{N-1}\left(\sqrt{t_m\bar{\lambda}}\right) & \text{under } \mathcal{H}_1\end{cases}.\tag{39}$$

where $I_a(x)=\sum_{k=0}^{\infty}(x/2)^{2k+a}/k!\Gamma(a+k+1)$, $x>0$ is the modified Bessel function of the first kind and order a.

With the above PDF expressions, the performance of the Rao test is given by

$$P_{\mathrm{fa},m}=\Pr\{T_R(z_m)>\gamma_{R_m}\,|\mathcal{H}_0\}=\int_{\gamma_{R_m}}^{\infty}p\left(t_m|\mathcal{H}_0\right)dt_m=\frac{\Gamma(N,\gamma_{R_m}/2)}{\Gamma(N)}\tag{40}$$

$$P_{\mathrm{d},m}=\Pr\{T_R(z_m)>\gamma_{R_m}\,|\mathcal{H}_1\}=\int_{\gamma_{R_m}}^{\infty}p(t_m|\mathcal{H}_1)\,dt_m=Q_N(\sqrt{\bar{\lambda}},\sqrt{\gamma_{R_m}})\tag{41}$$

where $\Gamma(u,v)=\int_v^\infty x^{u-1}e^{-x}\,dx, u,v>0$ is the upper incomplete gamma function, and $Q_N(\sqrt{u},\sqrt{u})=\int_v^\infty(1/2)(x/u)^{(N-1)/2}\exp(-(x+u)/2)I_{N-1}(\sqrt{xu})\,dx$, $u,v>0$ is the N-th order generalized Marcum's-Q function.

4.3. Asymptotic relative efficiency

The performance of the Rao detector with non-Gaussian noise for CR is now compared with the energy detector in terms of asymptotic relative efficiency (ARE). It is defined as the ratio of the numbers of data samples required to attain the given P_{fa} and P_{d} for two different test statistics when the sample size approaches infinity [25]. So the ARE of the test statistic T_{R_m} with respect to the test statistic T_{E_m} is defined as

$$ARE_{T_{Rm},T_{Em}}=\lim_{N\to\infty}\frac{N_{T_{Em}}}{N_{T_{Rm}}}\tag{42}$$

where $N\to\infty$ means that the data record length at hand is large enough to measure faithfully the energy or Rao test detection performance.

On the other hand, the detection performance can be characterized by the *deflection coefficient* d^2 for a detection statistic T, which gives an overall consideration of P_{fa} and P_{d}. The d^2 is given by [25]

$$d^2=\frac{(E\{T|\mathcal{H}_1\}-E\{T|\mathcal{H}_0\})^2}{\mathrm{var}\{T|\mathcal{H}_0\}}\tag{43}$$

In the case of energy detection, by substituting (27)–(29) into (43), the *deflection coefficient* of the energy detector is obtained as

$$\begin{aligned}d_{E_m}^2&=\frac{(E\{T_{E_m}|\mathcal{H}_1\}-E\{T_{E_m}|\mathcal{H}_0\})^2}{\mathrm{var}\{T_{E_m}|\mathcal{H}_0\}}\\&=\frac{N_{T_{Em}}\zeta_m^2}{\dfrac{\Gamma(1/\beta)\Gamma(5/\beta)}{\Gamma^2(3/\beta)}-1}\end{aligned}\tag{44}$$

In the case of Rao detection, using (39), the conditional mean and variance of $T_R(z_m)$ under $\mathcal{H}_0$ and under $\mathcal{H}_1$ are given by

$$E(T_R(z_m)|\mathcal{H}_0)=2N,\ \ \mathrm{var}\{T_Rz_m|\mathcal{H}_0\}=4N\tag{45}$$

$$E(T_R(z_m)|\mathcal{H}_1)=2N+\bar{\lambda},\ \ \mathrm{var}\{T_Rz_m|\mathcal{H}_0\}=4N+4\bar{\lambda}\tag{46}$$

and the *deflection coefficient* of Rao detection is thus obtained as

$$\begin{aligned}d_{R_m}^2&=\frac{(E\{T_{R_m}|\mathcal{H}_1\}-E\{T_{R_m}|\mathcal{H}_0\})^2}{\mathrm{var}\{T_{R_m}|\mathcal{H}_0\}}\\&=\frac{N_{T_{Rm}}\zeta_m^2[\beta(\beta-1)\Gamma(1-1/\beta)\Gamma(3/\beta)]^2}{\Gamma^4(1/\beta)}\end{aligned}\tag{47}$$

Accordingly, when the two detectors have the same detection performance, i.e., $d_{E_m}^2=d_{R_m}^2$, the $ARE_{T_{Rm},T_{Em}}$ is given by

$$ARE=\frac{[\beta(\beta-1)\Gamma(1-1/\beta)\Gamma(3/\beta)]^2}{\Gamma^4(1/\beta)}\left(\frac{\Gamma(1/\beta)\Gamma(5/\beta)}{\Gamma^2(3/\beta)}-1\right)\tag{48}$$

From (48), we know that the ARE for the two detectors depends only on the GGD shape factor β. As will be shown by simulations, the ARE increases with decreasing β. Moreover, our proposed Rao detector not only has a much better performance than the energy detector for all $\beta\in(0,2]$, but

also has an increasingly higher performance than the energy detector when the degree of non-Gaussianity increases.

5. Cooperative spectrum sensing with decision fusion

Each cognitive user needs to conduct the MLE of σ_w^2 and the Rao detection locally, yielding local decision results $\boldsymbol{y}=[y_1,y_2,\ldots,y_M]$ to be used by the FC. We assume that the decision device of the fusion center is implemented with the k-out-of-M rule, which means that the FC decides the presence of PU if there are k or more SUs that individually decide the presence of PU. The global decision of the FC is then given as

$$T_{FC}(y)=\sum_{m=1}^{M} y_m \underset{\mathcal{H}_0}{\overset{\mathcal{H}_1}{\gtrless}} \gamma_{FC} \tag{49}$$

where $\gamma_{FC}=1,2,\ldots,M$ is the decision threshold at the FC, and may be set to two extreme values: 1 (OR rule) and M (AND rule). In this paper, we generally assume γ_{FC} to be one of $1,2,\ldots,M$.

5.1. Cooperative detection with error-free channel

If the reporting channels between the M SUs and the FC are error-free, the cooperative probability of detection and that of false alarm are, respectively, given by

$$\begin{aligned}P_{\mathrm{d},\gamma_{FC}}&=\sum_{i=\gamma_{FC}}^{M}\Pr\left\{\sum_{m=1}^{M}y_m=i|\mathcal{H}_1\right\}\\&=\sum_{i=\gamma_{FC}}^{M}\sum_{j=1}^{C(M,i)}\prod_{m=1}^{M}P_{\mathrm{d},m}^{y_{m,i,j}}(1-P_{\mathrm{d},m})^{1-y_{m,i,j}},\end{aligned} \tag{50}$$

and

$$\begin{aligned}P_{\mathrm{fa},\gamma_{FC}}&=\sum_{i=\gamma_{FC}}^{M}\Pr\left\{\sum_{m=1}^{M}y_m=i|\mathcal{H}_0\right\}\\&=\sum_{i=\gamma_{FC}}^{M}\sum_{j=1}^{C(M,i)}\prod_{m=1}^{M}P_{\mathrm{fa},m}^{y_{m,i,j}}(1-P_{\mathrm{fa},m})^{1-y_{m,i,j}}\end{aligned} \tag{51}$$

where $C(M,i)=M!/i!(M-i)!$ denotes the number of combinations for any i out of M SUs that decide the presence of PU. Note that for a fixed value of i, the j-th combination can be denoted as $\boldsymbol{y}_{m,i,j}=[y_{1,i,j},y_{2,i,j},\ldots,y_{M,i,j}]$, where $j=1,2,\ldots,C(M,i)$. If every SU achieves identical false alarm probability P_{fa} and detection probability P_{d}, (50) and (51) can be simplified as

$$P_{\mathrm{d},\gamma_{FC}}=\sum_{i=\gamma_{FC}}^{M}C(M,i)P_{\mathrm{d}}^{i}(1-P_{\mathrm{d}})^{M-i} \tag{52}$$

and

$$P_{\mathrm{fa},\gamma_{FC}}=\sum_{i=\gamma_{FC}}^{M}C(M,i)P_{\mathrm{fa}}^{i}(1-P_{\mathrm{fa}})^{M-i} \tag{53}$$

respectively.

5.2. Cooperative detection with erroneous channel

If the channels between the SUs and the FC are imperfect, errors occur on the decision bits $\boldsymbol{y}$ which are transmitted by the SUs to the FC. Assuming a bit-by-bit transmission from SUs, each reporting channel can be modeled as a binary symmetric channel (BSC) with cross-over probability $p_{\mathrm{e},m}$. Denoting y_m' as the reporting signal received at the FC from m-th SU, given the decision y_m, then we have $P(y_m'=1|y_m=0)=P(y_m'=0|y_m=1)=P_{\mathrm{e},m}$.

Considering the m-th SU, when the PU is present, the probability of the FC receiving bit $y_m'=1$ from the m-th SU includes: the probability $P_{\mathrm{d},m}(1-P_{\mathrm{e},m})$ when $y_m=1$ and the probability $(1-P_{\mathrm{d},m})P_{\mathrm{e},m}$ when $y_m=0$. On the other hand, when the PU is absent, the probability of the FC receiving bit $y_m'=1$ from the m-th SU includes: the probability $P_{\mathrm{fa},m}(1-P_{\mathrm{e},m})$ when $y_m=1$ and the probability $(1-P_{\mathrm{fa},m})P_{\mathrm{e},m}$ when $y_m=0$. With the same decision rule in (49), the cooperative probability of detection and that of false alarm with reporting errors are, respectively, given by

$$\begin{aligned}P_{\mathrm{d},\gamma_{FC}}&=\sum_{i=\gamma_{FC}}^{M}\Pr\left\{\sum_{m=1}^{M}y_m'=i|\mathcal{H}_1\right\}\\&=\sum_{i=\gamma_{FC}}^{M}\sum_{j=1}^{C(M,i)}\prod_{m=1}^{M'}(P_{\mathrm{d},m}')^{y_{i,j,m}}(1-P_{\mathrm{d},m}')^{1-y_{i,j,m}}\end{aligned} \tag{54}$$

and

$$\begin{aligned}P_{\mathrm{fa},\gamma_{FC}}&=\sum_{i=\gamma_{FC}}^{M}\Pr\left\{\sum_{m=1}^{M}y_m'=i|\mathcal{H}_0\right\}\\&=\sum_{i=\gamma_{FC}}^{M}\sum_{j=1}^{C(M,i)}\prod_{m=1}^{M}(P_{\mathrm{fa},m}')^{y_{i,j,m}}(1-P_{\mathrm{fa},m}')^{1-y_{i,j,m}}\end{aligned} \tag{55}$$

where $P_{\mathrm{fa},m}'=P_{\mathrm{fa},m}(1-P_{\mathrm{e},m})+(1-P_{\mathrm{fa},m})P_{\mathrm{e},m}$ and $P_{\mathrm{d},m}'=P_{\mathrm{d},m}(1-P_{\mathrm{e},m})+(1-P_{\mathrm{d},m})P_{\mathrm{e},m}$ denote the false alarm and detection probabilities of the m-th SU with BSC. The BSC's crossover probability $P_{\mathrm{e},m}$ can be taken as a constant value (e.g., 0.1, 0.01, 0.05), but for Rayleigh fading channel, it is given by [22]

$$P_{\mathrm{e},m}=\frac{1}{2}\left(1-\sqrt{\left(\frac{\overline{\zeta}_m}{1+\overline{\zeta}_m}\right)}\right) \tag{56}$$

where $\overline{\zeta}_m$ is the SNR of the reporting channel between the m-th SU and the FC.

6. Numerical and simulation results

In this section, simulation results are provided to illustrate the performances of the proposed detector and cooperative scheme in different situations.

6.1. Generation of the GGD noise

Let F_X be the cumulative distribution function (CDF) of a random variable X and F_X^{-1} be its inverse. It is well known that if F_X^{-1} can be directly evaluated, a large number of realizations of X can be obtained as $x_i=F_X^{-1}(g_i)$, where g_i $(i=1,2,\ldots,n)$ are random numbers uniformly distributed over $[0,1]$. If F_X^{-1} has a closed-form expression, this method can be applied efficiently, such as in the case of Laplacian distribution. However, generating the samples of a GGD is, in general, a quite complicated task. In our simulation, we use the three-step method [28] for the cases of GGD with $0<\beta<2$.

6.2. Energy detection

Assume that the primary user signal $s(n)$ is a zero-mean complex Gaussian random variable, and the noise is a zero-mean GGD noise. The receiver operation characteristics (ROC) are computed based on 5000 Monte Carlo runs and the sample size is set to $N=1000$. Fig. 2 shows the energy detection performances for GGD. When β decreases, the degree of non-Gaussianity of the GGD noise increases. Clearly, the performance under GGD noise is worse than that under WGN, and the detection performance gets worse with increasing the degree of non-Gaussianity of the noise.

6.3. Rao test detection

Assume that the primary user is a PSK signal, $s(n)=\cos\ \phi(n)+j*\sin\ \phi(n)$, $\phi(n)\in[0,2\pi)$. Simulations are carried out with $N=1000$ and $M=1$. The performance of the proposed detector against the GGD noise with $\beta=1.1$ is shown in Fig. 3 with comparison to that of the energy detection for GGD noises with the same degree of non-Gaussianity. It is seen that when SNR $=-15$ dB and $P_{fa}=0.1$, the probability of detection of our detector is 70%, but that of the energy detector is 20% only, which fails to meet the requirement of spectrum sensing. Again, Fig. 4 shows that our proposed detector has a better detection performance than the energy detector and the PCA detector [14] under almost all levels of SNR for $\beta=1.5$, and $N=1000$ with $P_{fa}=0.1$.

In Fig. 5, the ROC curves for the Rao detector and the energy detector for different β are shown for SNR $=-20$ dB, $N=1000$. It further shows that for small values of β, Rao detector's performance is much better, even in very small SNR regions, than the energy detector.

In Fig. 6, the probabilities of detection of the Rao detector, the energy detector and the PCA detector are shown as a function of the shape parameter β of the GGD noise for SNR $=-20$ dB, -15 dB. The numerical results are obtained from the expressions (41) and (34), and equation (12) in [14]. It can be seen from Fig. 6 that as the degree of non-Gaussianity increases (β decreases), the

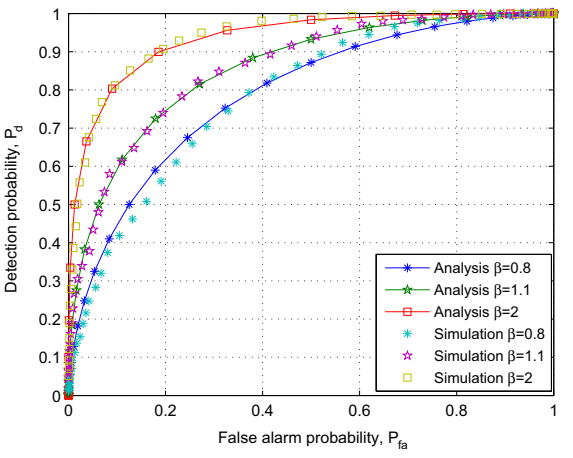

Fig. 2. ROC of energy detection for GGD at SNR $=-10$ dB.

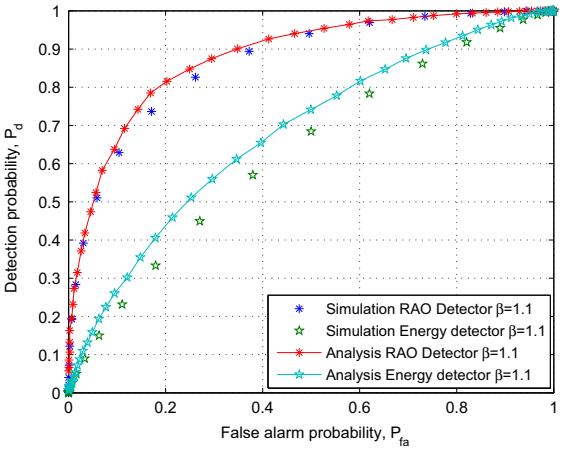

Fig. 3. ROC comparison of Rao detection and energy detection for GGD noise.

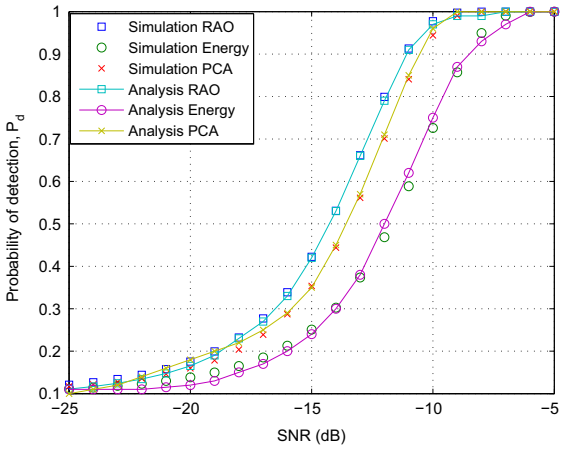

Fig. 4. Probability of detection vs. SNR with Rao detector, energy detector and PCA detector for GGD ($\beta=1.5$, $N=1000$, $P_{fa}=0.1$).

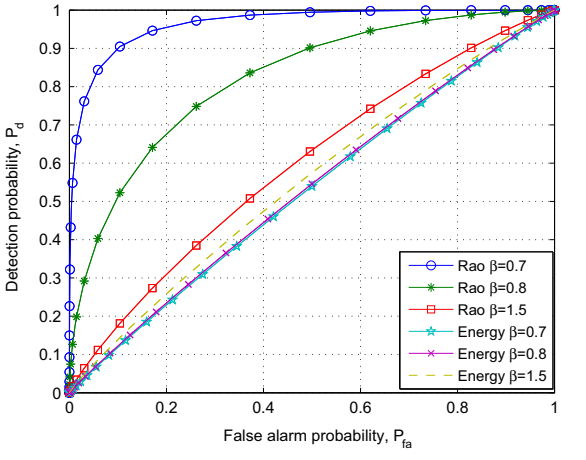

Fig. 5. ROC of Rao detector and energy detector for the GGD noise (SNR $=-20$ dB, $N=1000$).

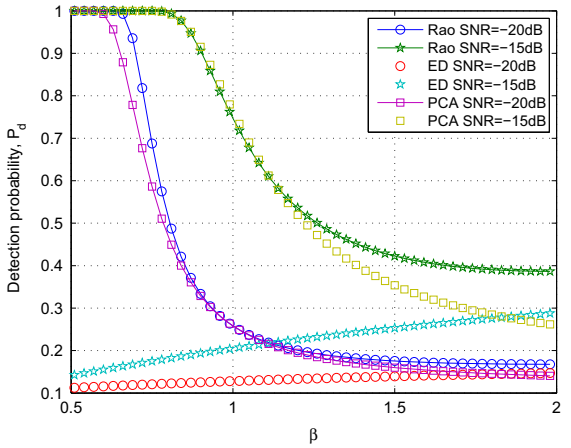

Fig. 6. Probability of detection vs. β for GGD noise ($P_{\text{fa}}=0.1$, $N=1000$).

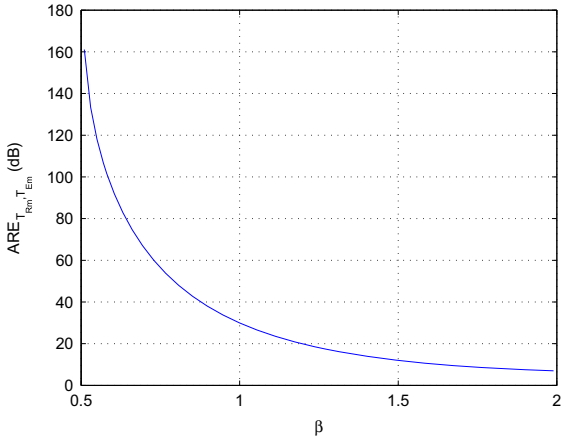

Fig. 7. $ARE_{T_{Rm},T_{Em}}$ vs. β for GGD noise.

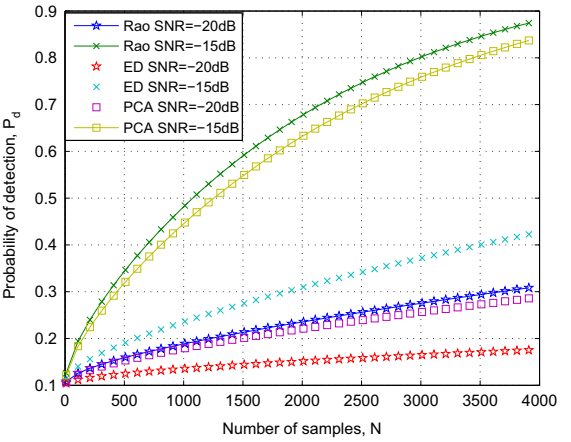

Fig. 8. Probability of detection vs. number of samples for GGD noise, $\beta=1.3$, $P_{\text{fa}}=0.1$.

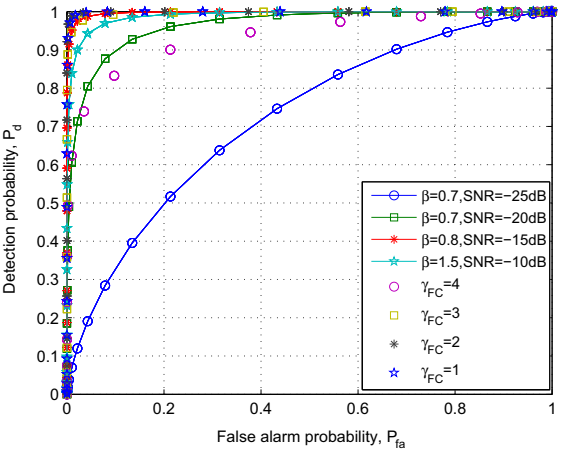

Fig. 9. ROC comparison of non-cooperative and cooperative performances over error-free reporting channels.

performance of the energy detector decreases while the performances of the Rao detector are greatly improved. We also see that the performance of the PCA detector is lower than that of our proposed detector when $\beta\in[1.2,2]$ and our proposed detector has better performance than the energy detector for all $\beta\in(0,2]$, while the performance of the PCA detector is lower than that of the energy detection when β close to 2. Fig. 7 shows that the ARE of the Rao detector with respect to the energy detector increases significantly as β decreases.

In Fig. 8, the performances of the Rao detector, the energy detector and the PCA detector versus the number of samples are shown for $\beta=1.3$, and $P_{\text{fa}}=0.1$. It can be seen that, for the same probability of detection, the number of samples required by the Rao detector is lower than that of the PCA detector and much lower than that of the energy detector, which is in accordance with the ARE illustrated in Fig. 7.

6.4. Cooperative detection

In cooperative detection, we assume that the number of observations is $N=1000$, and the number of SUs is $M=4$. We consider four different degrees of non-Gaussianity for the four SUs, namely, $\beta_1=0.7$, $\beta_2=0.7$, $\beta_3=0.8$ and $\beta_4=1.5$. The corresponding SNRs are assumed as -25 dB, -20 dB, -15 dB, and -10 dB.

Fig. 9 shows the ROC curves for the non-cooperative and cooperative detectors based on the Rao detection over error-free reporting channels. As shown in Fig. 9, when $P_{\text{fa}}=0.1$, the OR rule ($\gamma_{FC}=1$) results in the best performance, improving the worst probability of local detection from 30% ($\beta=0.7$, $\text{SNR}_1=-25$ dB) to 100%, while the AND rule ($\gamma_{FC}=4$) has the worst performance in all cooperative rules.

Fig. 10 indicates that the cooperative detection performance based on the Rao detector is much better than that using the energy detector. Further, in the energy based cooperative detection, the Majority rule ($\gamma_{FC}=2$) has the best probability of detection when $P_{\text{fa}}<0.4$, but for $0.4<P_{\text{fa}}<1$, the OR rule ($\gamma_{FC}=1$) results in the best performance.

Fig. 11 gives the ROC curves for the non-cooperative and cooperative detectors based on the Rao detection over erroneous reporting channels, where the cross-over

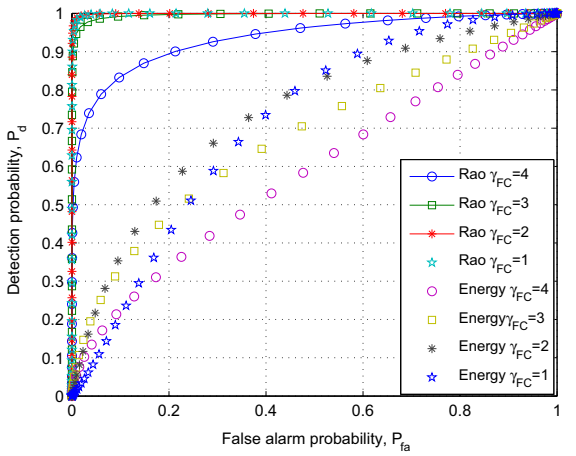

Fig. 10. ROC comparisons of Rao-based and energy-based cooperation with k-out-of-M rules over error-free reporting channels.

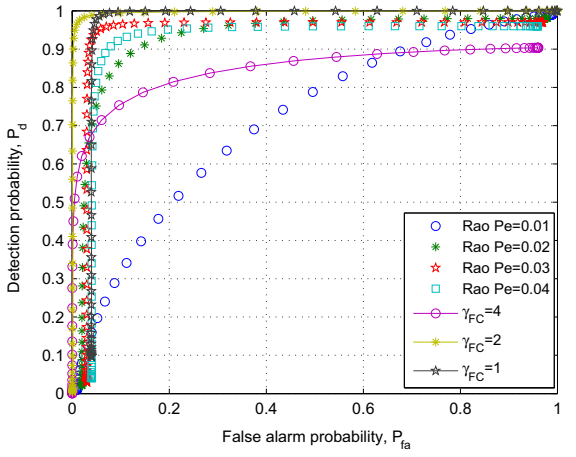

Fig. 11. ROC comparison of non-cooperative and cooperative performances over erroneous reporting channels.

probability P_e for the four SUs is assumed as $P_{e,1}=0.01, P_{e,2}=0.02, P_{e,3}=0.03$, and $P_{e,4}=0.04$. From Figs. 9 and 11, we can see that the detection performance decreases over erroneous reporting channels, especially, the probability of detection of the 4-th SU ($\beta_4=1.5$, $\mathrm{SNR}_4=-10$ dB) decreases from 100% to 95% when $P_{e,4}=0.04$, and $P_{fa}=0.2$. Fig. 11 also shows that the performances of the OR rule and the Majority rules decay at a higher threshold γ_R, but they are better than that of the AND rule for small values of γ_R. Note that because of the erroneous reporting, we do not have $(P_{fa},P_d)=(1,1)$ at $\gamma_R=0$ and $(P_{fa},P_d)=(0,0)$ at $\gamma_R=\infty$ on the ROC plot.

Fig. 12 shows the ROC curves for the cooperative detection based on the Rao detector over the Rayleigh fading reporting channels. We assume that the SNRs of the four reporting channels to be identical with $\hat{\zeta}=5$ dB or 3 dB. Fig. 12 shows that the performances of the three fusion rules vary with $\hat{\zeta}$. Further, for the same SNR of the Rayleigh fading reporting channels, the performance of the OR rule decays faster than that of the Majority rules at a higher threshold. Therefore, the Majority rule instead of the OR rule should be used to obtain the lower P_{fa} with the cooperative sensing over the Rayleigh fading reporting channels.

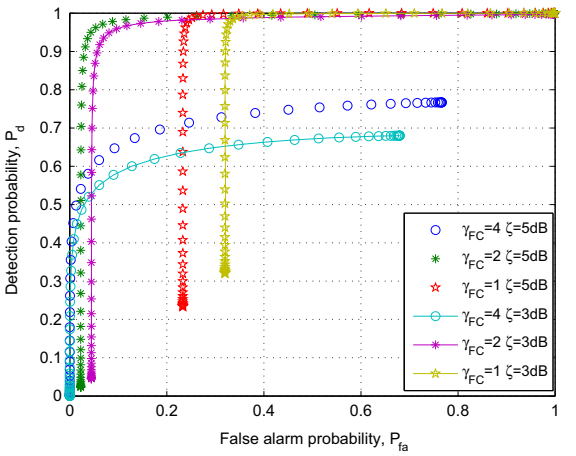

Fig. 12. ROC comparison of performances with k-out-of-M rules over with Rayleigh fading channels.

7. Conclusion

We have studied cooperative spectrum sensing in non-Gaussian noise environment that is modeled by GGD. We have focused on a scenario where the PU signal, the channel gain and the noise variance are unknown to the CR users. A Rao test based detector has been proposed and its detection performance has been analyzed against the traditional energy detector and the PCA detector. A cooperative scheme for spectrum sensing over error-free and erroneous reporting channels in non-Gaussian noises has been proposed based on the Rao test detector and the "k-out-of-M" decision rule. Numerical and simulation results show that the proposed Rao detector gives a much better performance than the traditional energy detector does when β varies between 0 and 2, while its performance is better than that of the PCA for $\beta\in(1.2,2]$. It has also been shown that the cooperative scheme exhibits a very good detection performance even in very low SNR regions and with erroneous reporting.

Appendix A. Calculation of FIM $\boldsymbol{I}(\boldsymbol{\theta})$

Here, we compute the four submatrices of the FIM $\boldsymbol{I}(\boldsymbol{\theta})$ in (8) under $\mathcal{H}_0$. First, we calculate the upper-left block $\boldsymbol{I}_{rr}(\boldsymbol{\theta})$ under $\mathcal{H}_0$:

$$\boldsymbol{I}_{rr}\left(\hat{\boldsymbol{\theta}}_0\right)=-E\left[\nabla[\nabla\ln p(\boldsymbol{z}_m;\hat{\boldsymbol{\theta}}_0)]^T\right]=\frac{\beta(\beta-1)}{[B(\beta,\hat{\sigma}^2_{w_m}/2)]^\beta}E[\boldsymbol{F}_{rr}] \tag{57}$$

where $\boldsymbol{F}_{rr}$ is a $2N\times 2N$ diagonal matrix, i.e.,

$$\boldsymbol{F}_{rr}=\mathrm{diag}[|z_m^{\Re}(1)|^{\beta-2},\ldots,|z_m^{\Re}(N)|^{\beta-2},|z_m^{\Im}(1)|^{\beta-2},\ldots,|z_m^{\Im}(N)|^{\beta-2}] \tag{58}$$

Under $\mathcal{H}_0$, we have $z_m(n)=w_m(n)$, and also the real and imagery parts of $w_m(n)$ are IID. So we have $E[|z_m^{\Re}(n)|^{\beta-2}]=E[|z_m^{\Im}(n)|^{\beta-2}]$, $n=1,2,\ldots,N$. Let x be a random variable that has the same distribution as the real or imagery part of the GGD noise w. Then, (57) can be rewritten as

$$\boldsymbol{I}_{rr}\left(\hat{\boldsymbol{\theta}}_0\right)=\frac{\beta(\beta-1)E[|x|^{\beta-2}]}{[B(\beta,\hat{\sigma}^2_{w_m}/2)]^{\beta}}\mathcal{I}_{2N}. \tag{59}$$

We now calculate $E[|x|^{\beta-2}]$, namely,

$$\begin{aligned}E\left[|x|^{\beta-2}\right]&=\int_{-\infty}^{\infty}\frac{\beta\exp\left(-\dfrac{|x|^{\beta}}{[B(\beta,\sigma^2_{w_m}/2)]^{\beta}}\right)}{2B(\beta,\sigma/2)\Gamma(1/\beta)}|x|^{\beta-2}\,dx\\&=\frac{\beta}{B(\beta,\sigma/2)\Gamma(1/\beta)}\int_0^{\infty}\exp\left(-\frac{x^{\beta}}{[B(\beta,\sigma^2_{w_m}/2)]^{\beta}}\right)x^{\beta-2}\,dx\end{aligned} \tag{60}$$

By letting $C=1/[B(\beta,\sigma^2_{w_m}/2)]^{\beta}$ and $t=Cx^{\beta}$, we have $x=(t/C)^{1/\beta}$ and $dx=(1/C)^{1/\beta}(1/\beta)t^{(1/\beta-1)}\,dt$, and further

$$\begin{aligned}E\left[|x|^{\beta-2}\right]&=\frac{(1/C)^{(1-1/\beta)}}{B(\beta,\sigma/2)\Gamma(1/\beta)}\int_0^{\infty}\exp(-t)t^{(-1/\beta)}\,dt\\&=\frac{[B(\beta,\sigma^2_{w_m}/2)]^{(\beta-1)}}{B(\beta,\sigma^2_{w_m}/2)\Gamma(1/\beta)}\Gamma(1-1/\beta)\end{aligned} \tag{61}$$

In obtaining the second equation of (61), we have used the identity $\Gamma(a)=\int_0^{\infty}\exp(-t)t^{(a-1)}\,dt$. Finally, by substituting (61) into (59), we obtain

$$\begin{aligned}\boldsymbol{I}_{rr}\left(\hat{\boldsymbol{\theta}}_0\right)&=\frac{\beta(\beta-1)\Gamma(1-1/\beta)}{B^2(\beta,\hat{\sigma}^2_{w_m}/2)\Gamma(1/\beta)}\mathcal{I}_{2N}\\&=2/\hat{\sigma}^2_{w_m}\frac{\beta(\beta-1)\Gamma(1-1/\beta)\Gamma(3/\beta)}{\Gamma^2(1/\beta)}\mathcal{I}_{2N}\end{aligned} \tag{62}$$

Next, we calculate the upper-right block $\boldsymbol{I}_{rs}(\boldsymbol{\theta})$ under $\mathcal{H}_0$:

$$\boldsymbol{I}_{rs}\left(\hat{\boldsymbol{\theta}}_0\right)=-E\left[\frac{\partial[\nabla\ln p(\boldsymbol{z}_m;\hat{\boldsymbol{\theta}}_0)]}{\partial\theta_s}\right]=-\frac{\beta^2E[\boldsymbol{F}_{rs}]}{2[B(\beta,\sigma^2_{w_m}/2)]^{\beta}\sigma^2_{w_m}} \tag{63}$$

where $\boldsymbol{F}_{rs}$ is a $2N$-dimensional real vector,

$$\boldsymbol{F}_{rs}=[|z_m^{\Re}(1)|^{\beta-1},\ldots,|z_m^{\Re}(N)|^{\beta-1},|z_m^{\Im}(1)|^{\beta-1},\ldots,|z_m^{\Im}(N)|^{\beta-1}]^T$$

In a manner similar to obtaining (61), we can get

$$\begin{aligned}E\left[|x|^{\beta-1}\right]&=\frac{[B(\beta,\sigma^2_{w_m}/2)]^{\beta-1}}{\Gamma(1/\beta)}\int_0^{\infty}\exp(-t)t^0\,dt\\&=\frac{[B(\beta,\sigma^2_{w_m}/2)]^{\beta-1}}{\Gamma(1/\beta)}\end{aligned} \tag{64}$$

By substituting (64) into (63), we obtain

$$\boldsymbol{I}_{rs}\left(\hat{\boldsymbol{\theta}}_0\right)=-\frac{\beta^2\Gamma^{1/2}(3/\beta)}{2\hat{\sigma}^3_{w_m}\Gamma^{3/2}(1/\beta)}\mathbf{1}_{2N,1} \tag{65}$$

With some simple calculation, we can show that the down-left block $\boldsymbol{I}_{sr}(\boldsymbol{\theta})$ under $\mathcal{H}_0$ is given by

$$\boldsymbol{I}_{sr}\left(\hat{\boldsymbol{\theta}}_0\right)=-\frac{\beta^2\Gamma^{1/2}(3/\beta)}{2\hat{\sigma}^3_{w_m}\Gamma^{3/2}(1/\beta)}\mathbf{1}_{1,2N}=[\boldsymbol{I}_{rs}(\hat{\boldsymbol{\theta}}_0)]^T \tag{66}$$

Finally, we calculate the down-right block $\boldsymbol{I}_{ss}(\boldsymbol{\theta})$ under $\mathcal{H}_0$:

$$\begin{aligned}\boldsymbol{I}_{ss}\left(\hat{\boldsymbol{\theta}}_0\right)&=-E\left[\frac{\partial^2[\ln p(\boldsymbol{z}_m;\hat{\boldsymbol{\theta}}_0)]}{\partial^2\theta_s}\right]\\&=\left[\frac{(2\beta+\beta^2)E[|x|^{\beta}]}{2[B(\beta,\sigma^2_{w_m}/2)]^{\beta}}-1\right]N/\sigma^4_{w_m}\end{aligned} \tag{67}$$

Here, $E[|x|^{\beta}]$ can be calculated as

$$\begin{aligned}E\left[|x|^{\beta}\right]&=\int_{-\infty}^{\infty}\frac{\beta\exp\left(-\dfrac{|x|^{\beta}}{[B(\beta,\sigma^2_{w_m}/2)]^{\beta}}\right)}{2B(\beta,\sigma/2)\Gamma(1/\beta)}|x|^{\beta}\,dx\\&=\frac{[B(\beta,\sigma^2_{w_m}/2)]^{(\beta)}}{\Gamma(1/\beta)}\int_0^{\infty}\exp(-t)t^{1/\beta}\,dt\\&=\frac{[B(\beta,\sigma^2_{w_m}/2)]^{\beta}\Gamma(1+1/\beta)}{\Gamma(1/\beta)}\\&=\frac{[B(\beta,\sigma^2_{w_m}/2)]^{\beta}}{\beta}\end{aligned} \tag{68}$$

where we have used the identity $\Gamma(1+x)=x\Gamma(x)$ to get the last equation in (68). Using (68) into (67) gives

$$\boldsymbol{I}_{ss}\left(\hat{\boldsymbol{\theta}}_0\right)=\frac{N\beta}{2\hat{\sigma}^4_{w_m}}. \tag{69}$$

Appendix B. Calculation of $\mathrm{var}\{T_{E_m}|\mathcal{H}_1\}$ in (30)

For the energy detection, we have

$$\begin{aligned}\mathrm{var}\{T_{E_m}|\mathcal{H}_1\}&=E\left[\sum_{n=1}^{N}|z_m(n)|^2-E\{T_{E_m}|\mathcal{H}_1\}\right]^2\\&=E\left[\left(\sum_{n=1}^{N}|z_m(n)|^2\right)^2\right]-E^2\{T_{E_m}|\mathcal{H}_1\}\\&=\sum_{n=1}^{N}E[|z_m(n)|^4]+2\sum_{i\neq j}E[|z_m(i)|^2|z_m(j)|^2]-E^2\{T_{E_m}|\mathcal{H}_1\}\\&=\sum_{n=1}^{N}E[|z_m(n)|^4]-N(E[|u_m|^2]+\sigma_m^2)^2\end{aligned} \tag{70}$$

Under the low SNR assumption, we have $|u_m(n)|\ll|w_m(n)|$. By using a Taylor series expansion of the complex function $[|z_m(n)|^4]$ around $w_m(n)$, we can compute

$$\begin{aligned}E\left[|z_m(n)|^4\right]&=E\left[|u_m(n)+w_m(n)|^4\right]\\&=E\left[|w_m(n)|^4+u_m^{\Re}(n)\frac{\partial|w_m(n)|^4}{\partial w_m^{\Re}(n)}+u_m^{\Im}(n)\frac{\partial|w_m(n)|^4}{\partial w_m^{\Im}(n)}\right.\\&\quad+\frac{1}{2!}(u_m^{\Re}(n))^2\frac{\partial^2|w_m(n)|^4}{\partial^2 w_m^{\Re}(n)}+\frac{1}{2!}(u_m^{\Im}(n))^2\frac{\partial^2|w_m(n)|^4}{\partial^2 w_m^{\Im}(n)}\\&\quad\left.+u_m^{\Re}(n)u_m^{\Im}(n)\frac{\partial^2|w_m(n)|^4}{\partial w_m^{\Re}(n)\partial w_m^{\Im}(n)}+\cdots\right]\end{aligned} \tag{71}$$

By ignoring higher-order terms and noting that $u_m(n)$ has zero mean, we can obtain

$$\begin{aligned}E\left[|z_m(n)|^4\right]&\approx E\left[|w_m(n)|^4\right]+\frac{1}{4}E\left[|u_m(n)|^2\right]\\&\quad E\left(\frac{\partial^2|w_m(n)|^4}{\partial^2 w_m^{\Re}(n)}+\frac{\partial^2|w_m(n)|^4}{\partial^2 w_m^{\Im}(n)}\right)\end{aligned}$$

$$= E\left[|w_m(n)|^4\right] + \frac{1}{4}E\left[|u_m(n)|^2\right]16E\left[w_m^{\Re}(n)^2 + w_m^{\Im}(n)^2\right]$$
$$= E[|w_m(n)|^4] + 4E[|u_m(n)|^2]E[|w_m(n)|^2] \quad (72)$$

Therefore,

$$\mathrm{var}\{T_{E_m}|\mathcal{H}_1\} = N\left[\frac{\Gamma(1/\beta)\Gamma(5/\beta)\sigma_m^4}{\Gamma^2(3/\beta)} + 4E\left[|u_m|^2\right]\sigma_m^2 - (E[|u_m|^2] + \sigma_m^2)^2\right]$$
$$= N\left[\left(\frac{\Gamma(1/\beta)\Gamma(5/\beta)}{\Gamma^2(3/\beta)} - 1\right)\sigma_m^4 + 2E\left[|u_m|^2\right]\sigma_m^2 - E^2\left[|u_m|^2\right]\right] \quad (73)$$

References

[1] G. Ganesan, Y.G. Li, Cooperative spectrum sensing in cognitive radio—part I: two user networks, IEEE Trans. Wireless Commun. 6 (June) (2007) 2204–2213.

[2] Y.-C. Liang, G.Y. Li, Cognitive radio networking and communications: an overview, IEEE Trans. Vehicular Technol. 60 (September) (2011) 3386–3407.

[3] Y. Zeng, Y.-C. Liang, A.T. Hoang, R. Zhang, A review on spectrum sensing for cognitive radio: challenges and solutions, EURASIP J. Adv. Signal Process. 2010 (2010) 15.

[4] G. Bansal, M. Hossain, P. Kaligineedi, H. Mercier, C. Nicola, U. Phuyal, M. Rashid, K.C. Wavegedara, Z. Hasan, M. Khabbazian, V.K. Bhargava, Some research issues in cognitive radio networks, in: IEEE AFRICON, 2007.

[5] D. Middleton, Statistical–physical models of man-made radio noise—parts I and II, U.S. Department of Commerce Office Telecommunication, April 1974 and 1976.

[6] T. Taher, M. Misurac, J. LoCicero, D. Ucci, Microwave oven signal interference mitigation for Wi-Fi communication systems, in: Proceedings of IEEE Consumer Communications Networking Conference, January 2008.

[7] N.H. Lu, B.A. Eisenstein, Detection of weak signals in non-Gaussian noise, IEEE Trans. Inf. Theory 27 (1981) 755–771.

[8] L. Izzo, L. Paura, M. Tanda, Signal interception in non-Gaussian noise, IEEE Trans. Commun. 40 (June) (1992) 1030–1037.

[9] C. Corral, S. Emami, G. Rasor, Model of multi-band OFDM interference on broadband QPSK receivers, in: Proceedings of IEEE International Conference on Acoustics, Speech, Signal Processing (ICASSP), November 2005.

[10] Y. Chen, N.C. Beaulieu, Novel low-complexity estimators for the shape parameter of the generalized Gaussian distribution, IEEE Trans. Vehicular Technol. 58 (2009) 2067–2071.

[11] F. Moghimi, A. Nasri, R. Schober, Adaptive Lp-norm spectrum sensing for cognitive radio networks, IEEE Trans. Commun. 59 (July) (2011) 1934–1945.

[12] J. Lunden, S.A. Kassam, V. Koivunennull, Robust nonparametric cyclic correlation-based spectrum sensing for cognitive radio, IEEE Trans. Signal Process. 58 (2010) 38–52.

[13] Q. Li, Z. Li, J. Shen, R. Gao, A novel spectrum sensing method in cognitive radio based on suprathreshold stochastic resonance, in: Proceedings of IEEE International Conference on Communications (ICC), 2012.

[14] T. Wimalajeewa, P.K. Varshney, Polarity-Coincidence-Array based spectrum sensing for multiple antenna cognitive radios in the presence of non-Gaussian noise, IEEE Trans. Wireless Commun. 10 (2011) 2362–2371.

[15] S.J. Zahabi, A.A. Tadaion, Local spectrum sensing in non-Gaussian noise, in: Proceedings of IEEE International Conference on Telecommunications (ICT), March 2010.

[16] S.M. Kay, D. Sengupta, Detection in incompletely characterized colored on-Gaussian noise via parametric modeling, IEEE Trans. Signal Process. 41 (October) (1993) 3066–3070.

[17] D. Sengupta, S.M. Kay, Parameter estimation and GLRT detection in colored non-Gaussian autoregressive processing, IEEE Trans. Acoustics Signal Process. 38 (October) (1990) 1661–1676.

[18] S. Zarrin, T.J. Lim, Composite hypothesis testing for cooperative spectrum sensing in cognitive radio, in: Proceedings of IEEE International Conference on Communications (ICC), June 2009.

[19] A. Ghasemi, E. Sousa, Collaborative spectrum sensing for opportunistic access in fading environments, in: Proceedings of IEEE International Symposium on New Frontiers in Dynamic Spectrum Access Networks, Baltimore, Maryland, USA, November 2005.

[20] I.F. Akyildiz, B.F. Lo, R. Balakrishnan, Cooperative spectrum sensing in cognitive radio networks: a survey, Phys. Commun. 4 (2011) 40–62.

[21] W. Zhang, K.B. Letaief, Cooperative spectrum sensing with transmit and relay diversity in cognitive radio networks, IEEE Trans. Wireless Commun. 7 (December) (2008) 4761–4766.

[22] S. Atapattu, C. Tellambura, H. Jiang, Energy detection based cooperative spectrum sensing in cognitive radio networks, IEEE Trans. Wireless Commun. 10 (2011) 1232–1240.

[23] X. Zhu, B. Champagne, W.-P. Zhu, Cooperative spectrum sensing based on the Rao test in non-Gaussian noise environments, in: Proceedings of IEEE International Conference on Wireless Communications and Signal Processing (WCSP), 2013.

[24] S.A. Kassam, Signal Detection in Non-Gaussian Noise, Springer Verlag, 1988.

[25] S.M. Kay, Fundamentals of Statistical Signal Processing: Detection Theory, vol. II, Publishing House of Electronics Industry, 2003.

[26] S.M. Kay, Fundamentals of Statistical Signal Processing: Estimation Theory, vol. I, Publishing House of Electronics Industry, 2003.

[27] P.A. Horn, C.R. Johnson, Matrix Analysis, Cambridge University Press, 1985.

[28] M. Nardon, P. Pianca, Simulation techniques for generalized Gaussian densities, J. Statistical Comput. Simul. 79 (November) (2009) 1317–1329.